Supporting Information (SI) to

Self-association engineering in P123 micelles rationalizing the role of other Pluronics® with varying hydrophilicity as a mixed system

Nitumani Tripathi[a], Germán Pérez-Sánchez[b], Nicolas Schaeffer[b], Debes Ray[c], Vinod K. Aswal[c], Ketan Kuperkar [a,*], João A. P. Coutinho[b], Pratap Bahadur[d]

[a]*Department of Chemistry, Sardar Vallabhbhai National Institute of Technology (SVNIT), Ichchhanath, Surat, 395 007, Gujarat, INDIA.*
[b]*Department of Chemistry, CICECO, University of Aveiro 3810-193, Aveiro, PORTUGAL.*
[c] *Solid State Physics Division, Bhabha Atomic Research Centre (BARC), Trombay, Mumbai, 400 085, Maharashtra, INDIA.*
[d]*Department of Chemistry, Veer Narmad South Gujarat University (VNSGU), Udhana-Magdalla Road, Surat, 395 007, Gujarat, INDIA.*

***Corresponding author:** E-mail: ketankuperkar@gmail.com

Declaration of interest: None

Mathematical models for scattering data fitting

For spherical micelles (Q^{-4}), ellipsoidal micelles (Q^{-3}), rod-like (Q^{-1}), and vesicles (Q^{-2}), the differential scattering cross-section per unit volume ($d\Sigma/d\Omega$) corresponds to each morphology, reflecting their distinctive scattering behaviors.

For a spherical particle of radius *R*, *F*(*Q*) is given by

$$\mathrm{F(Q)} = \frac{\mathrm{Scale}}{\mathrm{V_s}}\left[\frac{3\mathrm{V_c}\,(\rho_c - \rho_s)\,\mathrm{j_i}\,(\mathrm{qR_c})}{\mathrm{qR_c}} + \frac{3\mathrm{V_s}\,(\rho_s - \rho_{solv})\,\mathrm{j_i}\,(\mathrm{qR_s})}{\mathrm{qR_s}}\right]^2 + \mathrm{B} \tag{1}$$

Where $\mathrm{j_i}\,(\mathrm{x}) = (\sin\mathrm{x} - \mathrm{x}\cos\mathrm{x})/\mathrm{x}^2$, $\mathrm{R_s} = \mathrm{R_c} + \mathrm{t}$ and $\mathrm{v_i} = (4\pi/3)\,\mathrm{r_i}^{3}$

For an ellipsoidal particle of radius *R*, *P*(*Q*) is given by

$$\mathrm{P(Q)} = \frac{\mathrm{Scale}}{\mathrm{V_{ell}}}(\rho_{ell} - \rho_{solv})^2 \int_0^1 \mathrm{f}^2\,[\mathrm{qR_b}\,(1 + \mathrm{x}^2(\mathrm{v}^2 - 1)^2]\mathrm{dx} + \mathrm{B} \tag{2}$$

where $\mathrm{f(z)} = 3\mathrm{V_{ell}}\,\frac{\sin z - z\cos z}{z^3}$; $\mathrm{V_{ell}} = \frac{4\pi}{3}\,\mathrm{r_a}\,\mathrm{r_b}^{2}$; $\mathrm{v} = \frac{\mathrm{r_a}}{\mathrm{r_b}}$

For a prolate ellipsoidal particle with semi-major and semi-minor axes *a* and *b*, respectively,

$$F(Q) = \int_0^1 F(Q,\mu)\,\mathrm{d}\mu \tag{3}$$

where $F(Q,\mu) = \frac{3(\sin x - x\cos x)}{x^3}$ (4)

$$x = Q\left[a^2\mu^2 + b^2(1-\mu^2)\right]^{1/2} \tag{5}$$

Here, μ in the above equation refers to cosine of the angle between the directions of *a* and *Q*.

For a rod-like micelle of length $L = 2l$ and cross-sectional radius *R*,

$$P(Q) = \int_0^{\pi/2} \frac{\sin^2(Ql\ \cos\beta)}{Q^2l^2\ \cos^2\beta}\,\frac{4J_1^2(QR\ \sin\beta)}{Q^2R^2\ \sin^2\beta}\sin\beta\ \mathrm{d}\beta \tag{6}$$

where β is the angle between the axis of the rod and bisectrix. J_1 is the Bessel function of order unity.

$$I(Q) = \frac{Scale}{V_{Shell}}\left[\frac{3V_1\,(\rho_1 - \rho_2)j_i(qR_1)}{qR_1} + \frac{3V_2\,(\rho_2 - \rho_{solv})j_i(qR_2)}{qR_2}\right]^2 + bkg \tag{7}$$

where the vesicle is best defined in terms of a core radius (= R_1) and a shell thickness, t. Then the radii R_1 and R_2 are defined as: $R_1 = R_{core}$; $R_2 = R_{core} + t$; $V_{Shell} = \frac{4\pi}{3}(R_2 - R_1)^3$; and $V_i = \frac{4\pi}{3}(R_i)^3$.

CG-MD simulation depicting self-association

P123

P123, being moderately hydrophobic, allows it to self-assemble into various nanoscale structures, including micelles, vesicles, and bilayers. The CG-MD simulation for 5 %w/v P123 was performed at two different temperatures: 30 °C and 70 °C (**Figure S1**). At higher temperatures, P123 tends to form more complex structures such as rod-like, vesicle, and hexagonal.[15,37,67] The numbers on the image represent different time points in the simulation. For instance, at 1.1 μs, P123 molecules are still in the process of assembling into the spherical structure. By 8.0 μs, the micelle is fully assembled and has reached equilibrium. **Figure S1** also shows ellipsoidal micellar morphology, which is more stable at 70 °C than at 30 °C. Such enhanced stability is further rationalized by considering the increased mobility of P123 molecules. Here, the kinetic energy associated with the higher temperatures facilitates the formation of ellipsoidal micelles, underscoring the temperature-dependent nature of P123 self-assembly, which is further validated by the SANS data presented in the main manuscript (**Figure 4b** and **Table 1**).

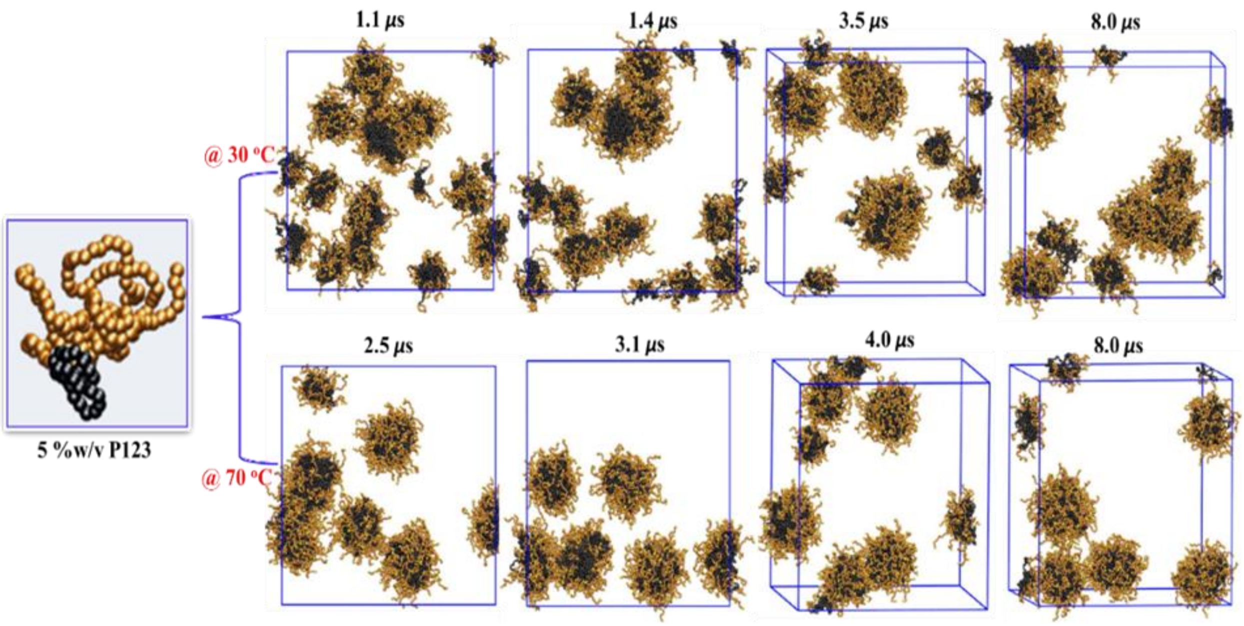

Figure S1: CG-MD simulation snapshots at different stages for the 5 %w/v P123 aqueous solution at 30 °C and 70 °C. The color code is as follows: EO and PO in the P123 are orange and black, respectively.

Relative solution viscosity (η_{rel})

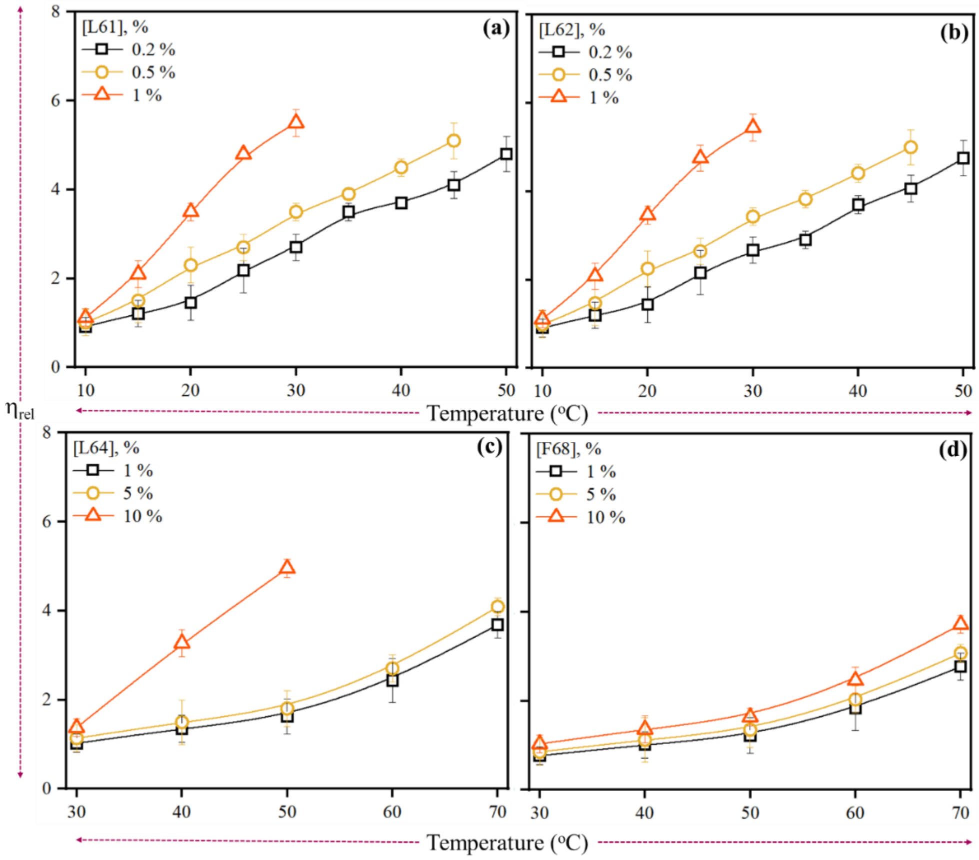

Figure S2: Relative viscosity (η_{rel}) of Pluronics® (a) L61, (b) L62, (c) L64, and (d) F68 measured at various concentrations as a function of temperature. The standard deviation of the measured η_{rel} values is within ±0.5.

Scattering profile

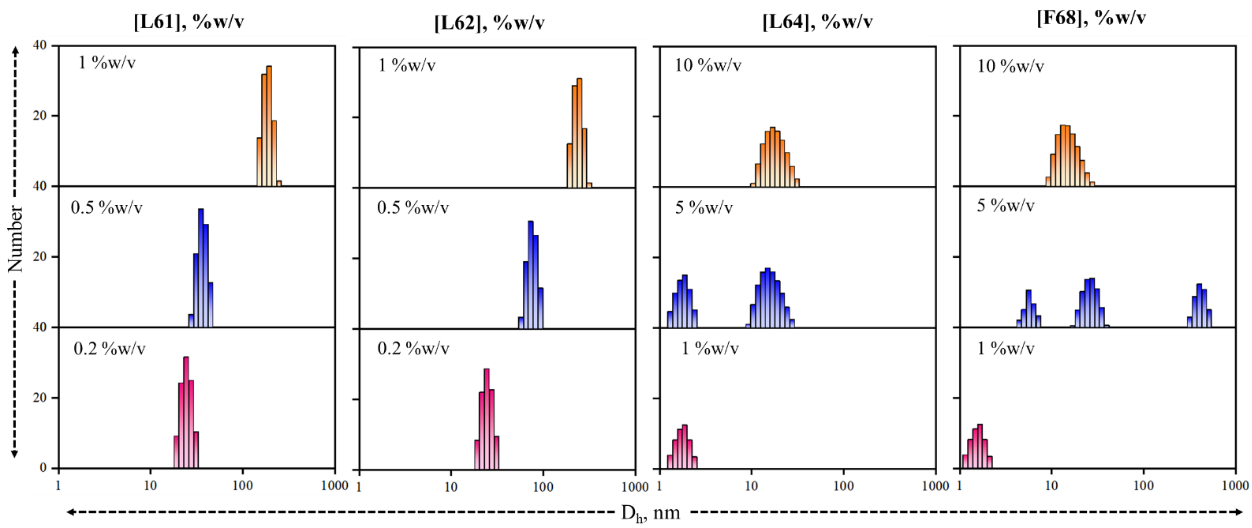

Figure S3: Size distribution profiles obtained from DLS measurements for different Pluronics® L61, L62, L64, and F68 at varying concentrations at 30 °C.

CG-MD simulation

L61

The hydrophobic character of L61 (10 %EO content) was noticed in its phase behavior at different concentrations, as shown in **Figure S4a**. Here, 0.2 %w/v L61 solution displayed BP ~ 30-37 ^{o}C and progressively undergo 2ϕ ~38 ^{o}C. Upon increasing the concentration to 0.5 %w/v of L61, the BP and CP appeared earlier than 0.2 %w/v, indicating a rapid tendency to form micelles and 2ϕ while the 1 %w/v L61 solution displayed an unstable BP ~23 ^{o}C and 2ϕ ~25 ^{o}C. The relative viscosity (η_{rel}) increases significantly with temperature, with a more gradual rise observed at lower concentrations (0.2 %w/v and 0.5 %w/v) (**Figure S2a**). At higher concentrations (1%w/v), the increase in the structural changes within the micellar network becomes more pronounced due to the enhanced micelle-micelle interactions. Such observed instability implies a disturbance in the self-assembly process of L61 molecules into micelles, potentially caused by the saturation of hydrophobic contacts that affect the thermodynamic equilibrium of L61. Here, the D_h was obtained ~24.7 nm, ~34.6 nm, and ~306.1 nm for 0.2 %w/v, 0.5 %w/v, and 1 %w/v L61, respectively, at 30 °C (**Figure S3**). This progressive increase in micellar size indicates enhanced micellar aggregation and structural transitions, driven by increasing concentration. Furthermore, 1 %w/v L61 displayed unilamellar vesicular (ULV) structure with a radius of vesicle (R_v) ~7.06 nm and thickness of vesicle (t_v) ~1.22 nm. This observation aligns with the findings previously reported by our group[6] and is corroborated by earlier studies.[63,64]

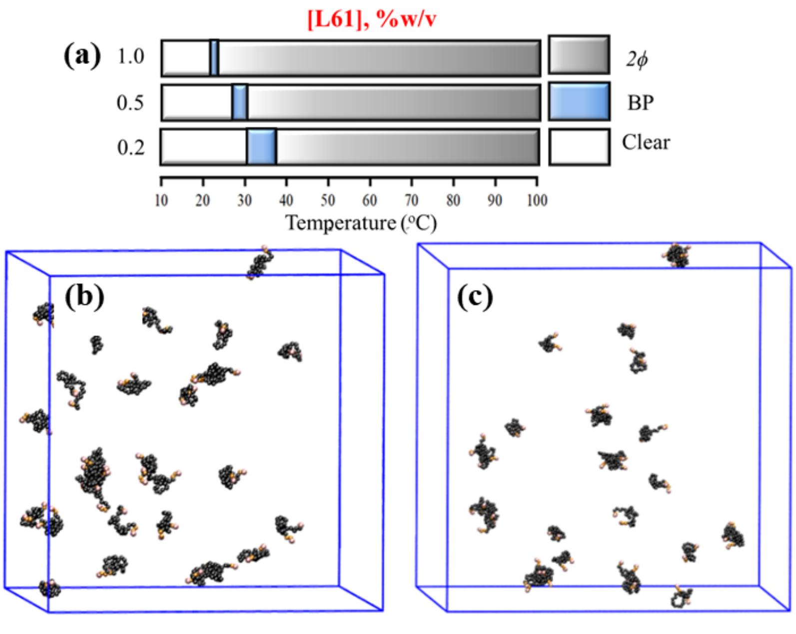

Figure S4: (a) Experimental solution behavior of L61 with varying concentration as a function of temperature, the CG-MD simulation snapshot for (b) 0.2 %w/v of L61 at 30 ^{o}C and (c) for the 0.5 %w/v of L61 solution at 35 ^{o}C after 20000 ns of simulation time. The color code in (b) and (c) is as follows: EO and PO groups were colored in orange and black, respectively, whereas water molecules were removed for clarity.

However, the ULV observed in our experiments is in contrast with the small L61 aggregates and monomers obtained in the CG-MD simulations (**Figures S4b** and **S4c**). Unfortunately, the low concentration of L61 dramatically increased the computational cost, and the equilibrium could not be assessed even after 20000 ns of simulation time.

L62

L62, which contains 20 %EO content, displays hydrophobic characteristics. The experimental phase behavior results in water at different concentrations, as shown in **Figure S5a**. Here, the clouding behavior was similar to L61 but with a noticeable temperature delay (**Figures S4a** and **S5a**). Even so, the effectiveness of L62 in inducing phase behavior is comparatively lower than L61, as expected from the more hydrophilic character of L62. The η_{rel} also increases with temperature and concentration but less steeply compared to L61. Consequently, the micellization and η_{rel} rise are less dramatic at lower concentrations (**Figure S2b**). At 1 %w/v, the formation of a micellar network becomes more significant, leading to a noticeable increase in η_{rel}. The D_h for L62 was obtained ~ 22.5 nm, ~40.2 nm, and ~280.7 nm for 0.2 %w/v, 0.5 %w/v, and 1 %w/v, respectively, at 30 °C (**Figure S3**). Conversely, the relatively smaller D_h values for L62 than L61 suggest a slower rate of micelle aggregation, reflecting its lower PO content. **Figures S5b** and **S5c** displayed the simulation snapshots after 20 μs, where only small aggregates were found, highlighting the difficulty of reaching a proper equilibrium for the L62 and L61 solutions under diluted conditions.

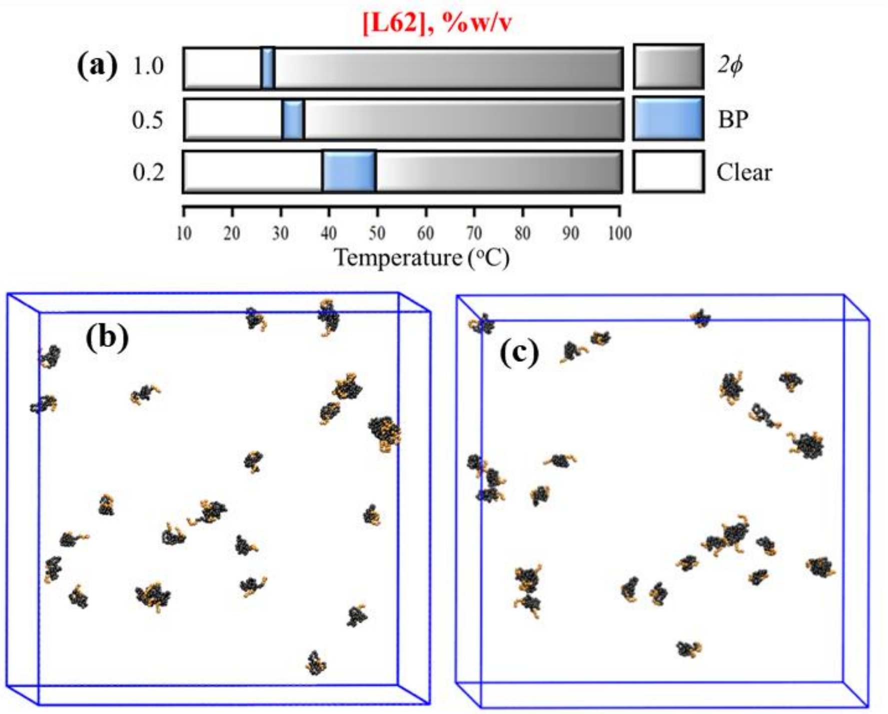

Figure S5: (a) Experimental solution behavior of L62 with varying concentration as a function of temperature, (b) and (c) CG-MD simulation snapshots after 20000 ns of simulation time for the 0.2 %w/v of L62 aqueous solution at 30 °C and 45 °C respectively. The color code is as follows: the EO and PO groups were colored in orange and black, respectively, and water molecules in the simulation snapshots were removed for clarity.

L64

The solution behavior of moderately hydrophobic L64, possessing 40 %EO content, was evaluated in water with varying concentrations, as depicted in **Figure S6a.** 1 %w/v L64 showed an unstable BP ~66-68 ^oC. Still, upon further heating, the 2ϕ appeared at ~69 ^oC. Conversely, when the concentration is increased to 5 %w/v, the L64 solution displays the BP and CP at ~64-66 ^oC and ~68 ^oC, respectively. The η_{rel} increases with concentration and temperature, but the rise is more gradual compared to L61 and L62, even at higher concentrations such as 10 %w/v (**Figure S2c**). L64 has a more balanced ratio of EO to PO, leading to a slower and more gradual micellization process. The D_h of 1 %w/v L64 was ~1.8 nm at 30 ^oC, corresponding to the unimer (**Figure S3**). For 5 %w/v L64, a similar unimer peak (D_h∼1.8 nm) was observed, along with a distinct micellar peak at ~14.6 nm at 30 °C. With a further increase in concentration to 10 %w/v, the micellar size grew slightly, with D_h increasing from ~14.6 nm to ~16.9 nm at 30 °C highlighting the emergence and growth of micellar aggregates as concentration increases. The findings at 10 %w/v L64 were similar, displaying spherical micelles with an average D_h of ~14-16 nm, as reported in the literature.[5,7] CG-MD simulations for 5 %w/v L64 aqueous solution at 30 ^oC and 70 ^oC were carried out over 8.0 μs of simulation time. It can be noticed that L64 micelles were formed at both temperatures, spherical at 30 ºC and prolate-shaped at 70 ºC as shown in **Figures S6b** and **S6c**, respectively. The micelle shape is observed in the density profiles displayed in **Figures S6d** and **S6e** for the solutions at 30 ºC and 70 ºC, respectively. The L64 micelles at 70 ºC displayed a higher and flatter density profile (black line), denoting a prolate-shaped micelle core (micelle corona radius ~3.0 nm, denoted by the maximum of the EO groups shown in orange), whilst the profile for the spherical L64 micelles is more symmetric and denotes a smaller radius ~2.4 nm. **Figures S6f** and **S6g** display the SASA profiles highlighting the dehydration of both PO and EO L64 groups when the temperature is increased from 30 ºC to 70 ºC. The initial decrease in SASA (first 500 ns) conveyed the fast formation of L64 early micelles, which grow smoothly throughout micelle fusion processes, as denoted by the constant value of the EO and PO SASA profiles at both temperatures (> 1000 ns). **Figure S6f** also denotes the increased dehydration of EO groups (L64 micelle corona) at 70 ºC compared to the L64 micelles at 30 ºC. Interestingly, as illustrated in **Figure S6g**, PO groups of L64 micelles at 70 ºC were more hydrated than their counterparts at 30 ºC. This points out directly the fact that prolate-shaped micelle cores exhibit a higher PO core when compared with the spherical cores of L64 micelles at 30 ºC.

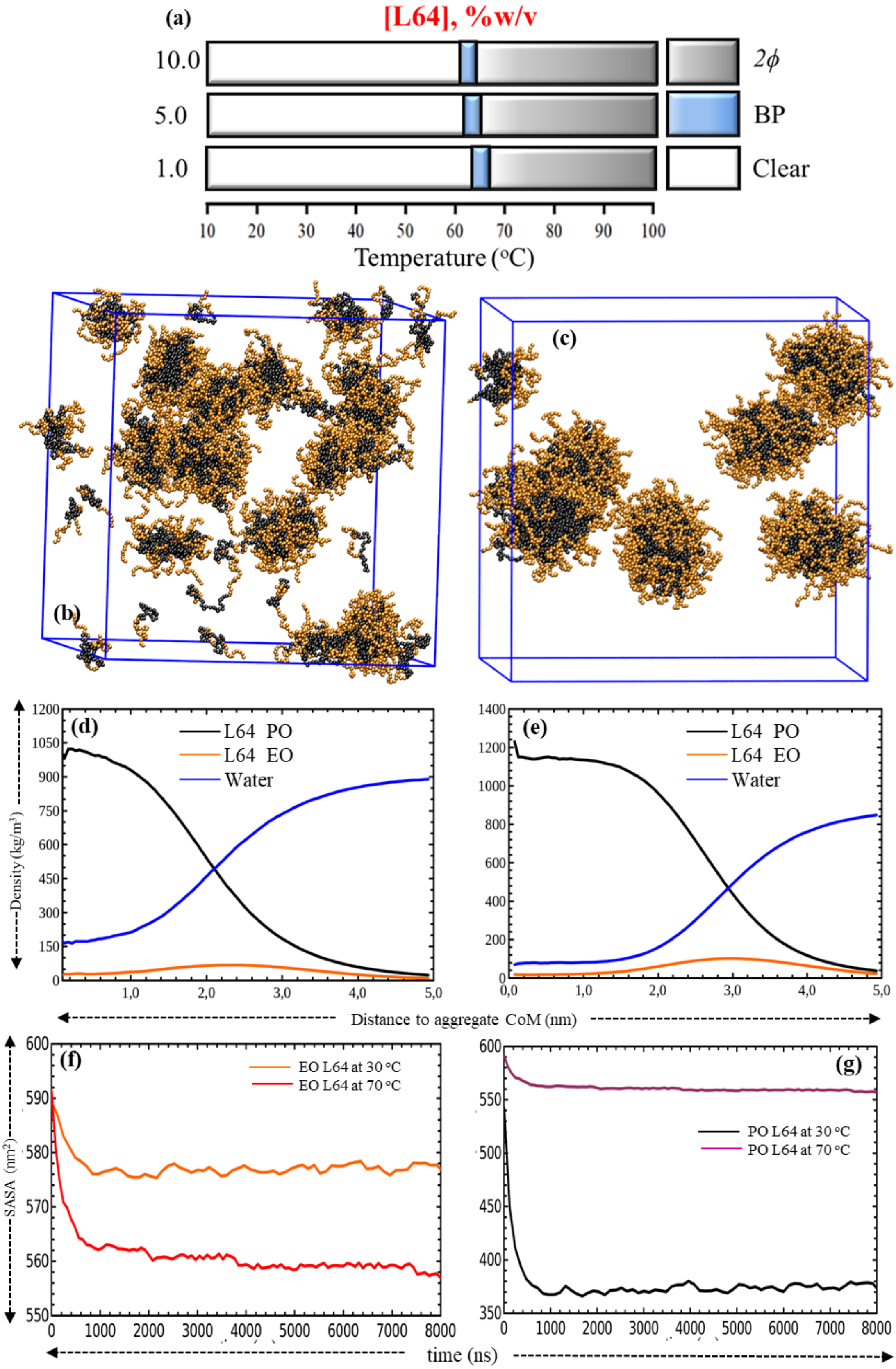

Figure S6: (a) Solution behavior of L64 as a function of concentration and temperature. (b) and (c) CG-MD simulation snapshots after 8000 ns of simulation time for the 5 %w/v of P123 aqueous solution at 30 °C and 70 °C, respectively. (d) and (e) density profiles of the obtained micelles taking its centre of mass (CoM) as reference. The color code is as follows: the EO and PO groups were colored in orange and black, respectively. The water molecules in the simulation snapshots (a) and (b) were removed for clarity. EO and PO groups SASA profiles are displayed in (f) and (g), respectively.

F68

The F68, entailing 80 %EO content, is highly hydrophilic, yielding CP > 100ºC, thus, the phase separation 2ϕ was not observed as denoted in **Figure S7a,** exhibiting a clear solution sample in the tested concentrations and temperatures. The η_{rel} shows the smallest increase among the examined copolymers, even at high concentrations (10 %w/v), as depicted in **Figure S2d**, and elevated temperatures due to a low PO fraction and the strong hydration of EO blocks. The D_h for 1 %w/v F68 exhibited a unimer peak at ~1.64 nm at 30 °C (**Figure S3**). With increasing concentration, at 5 %w/v F68, the D_h showed a unimer peak at ~5.5 nm, a micelle size of ~26.8 nm, with the presence of clusters (~406.1 nm) at 30 °C. At a higher concentration of 10 %w/v, showed complete micellization with a D_h of ~16.4 nm at 30 °C. These findings indicate a progression from unimers to micelles and clusters as the concentration increases, with complete micellization occurring at 10 %w/v.

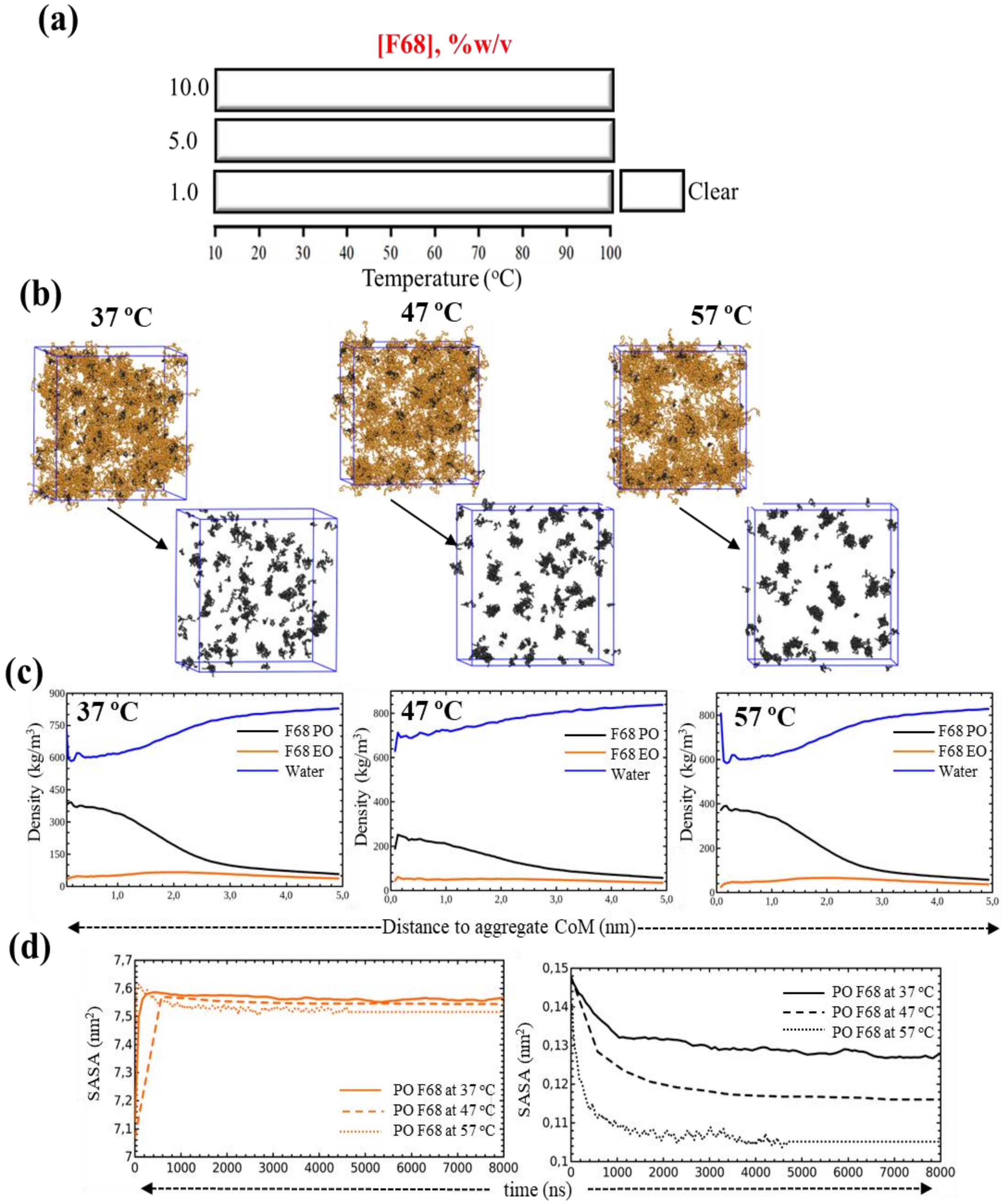

Figure S7: (a) Experimental solution behavior of F68 with varying concentration as a function of temperature. (b) CG-MD simulation snapshots for 5 %w/v F68 at 37 °C, 47 °C, and 57 °C, respectively, where insets show F68 without EO groups to highlight the distribution of small aggregates and unimers. (c) density profiles denoting the lack of noticeable aggregates. d) SASA profiles for PO and EO F68 groups along 8000 ns of simulation (water molecules were removed in the simulation snapshots for clarity). The color code is as follows: EO and PO groups of F68 are colored in orange and black, respectively. The SASA for PO and EO are shown in black and orange, respectively with solid, dashed, and dotted lines denoting the results for 30 °C, 47 °C, and 70 °C temperatures, respectively.

In fact, CG-MD simulations for 5 %w/v F68 showed no noticeable aggregates, as can be seen in the simulation snapshots shown in **Figure S7b**. Small aggregates and unimers were found at 37 ºC, 47 ºC, and 57 ºC. **Figure S7c** denotes flattening density profiles, highlighting the lack of micelles. SASA for EO and PO groups of F68 is displayed in **Figure S7d**, illustrating the expected dehydration of PO groups when the temperature is increased from 37 ºC to 57 ºC, barely denoting a minimal degree of self-assembly. The initial decrease in all profiles (first 2000 ns) denotes a weak aggregation, then grows smoothly (basically by micelle fusion processes), remaining stable (~ 7000 ns) until the end of the simulation (**Figure S7)**. However, the dehydration of EO groups was less pronounced than that of PO groups in a solution predominantly composed of unimers, which was consistent with expectations. The higher hydrophilicity of EO groups results in a diminished propensity for EO groups to undergo dehydration when the temperature increases.

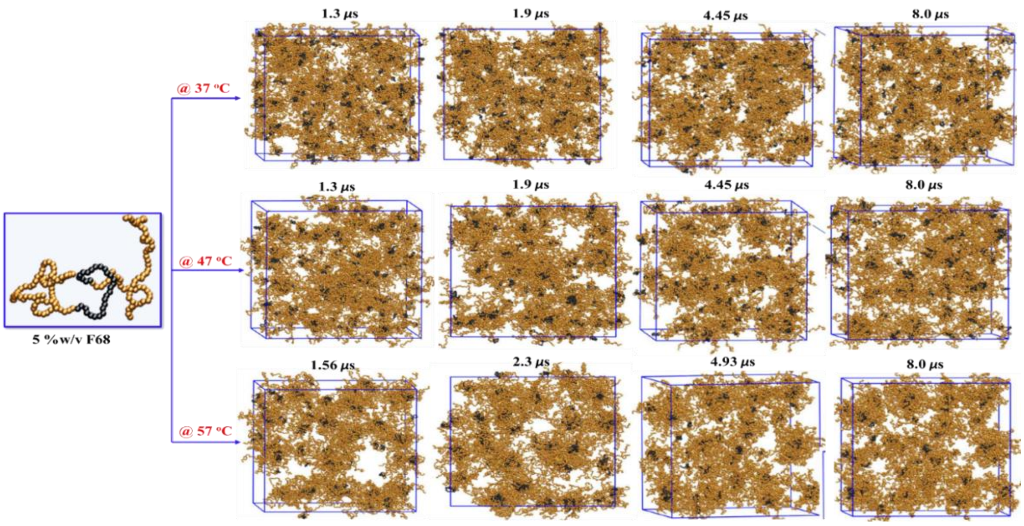

Figure S8: CG-MD simulation snapshots at different stages for the 5 %w/v F68 as a function of temperature. The color code is as follows: PEO and PPO in the F68 are in orange and black, respectively.

Figure S8 demonstrates the self-assembly process of 5 %w/v F68 molecules. Initially dispersed in water, F68 molecules, characterized by 80 %EO composition (highly hydrophilic), exhibit a tendency to be unimers. Over the time, these molecules undergo a process of growth, leading to the enlargement of micelles, ultimately culminating in their fusion to form a singular spherical structure. The molecular events captured in the figure unfold as follows: At 1.3 μs, F68 molecules are dispersed in water. By 1.9 μs, the monomers have grown in size and are initiating the process of fusion. Progressing to 4.45 μs, the monomers have successfully fused, endeavouring to establish a unified, spherical micelle. At 8.0 μs, equilibrium is attained, with the monomers fully amalgamated into a cohesive structure. At higher temperatures, F68 molecules exhibit increased mobility and greater energy, facilitating the surmounting of energy barriers associated with coalescence. This temperature-dependent behavior underscores the dynamic interplay between molecular motion, energy, and the resulting coalescence process in F68 self-assembly.

Apparent viscosity

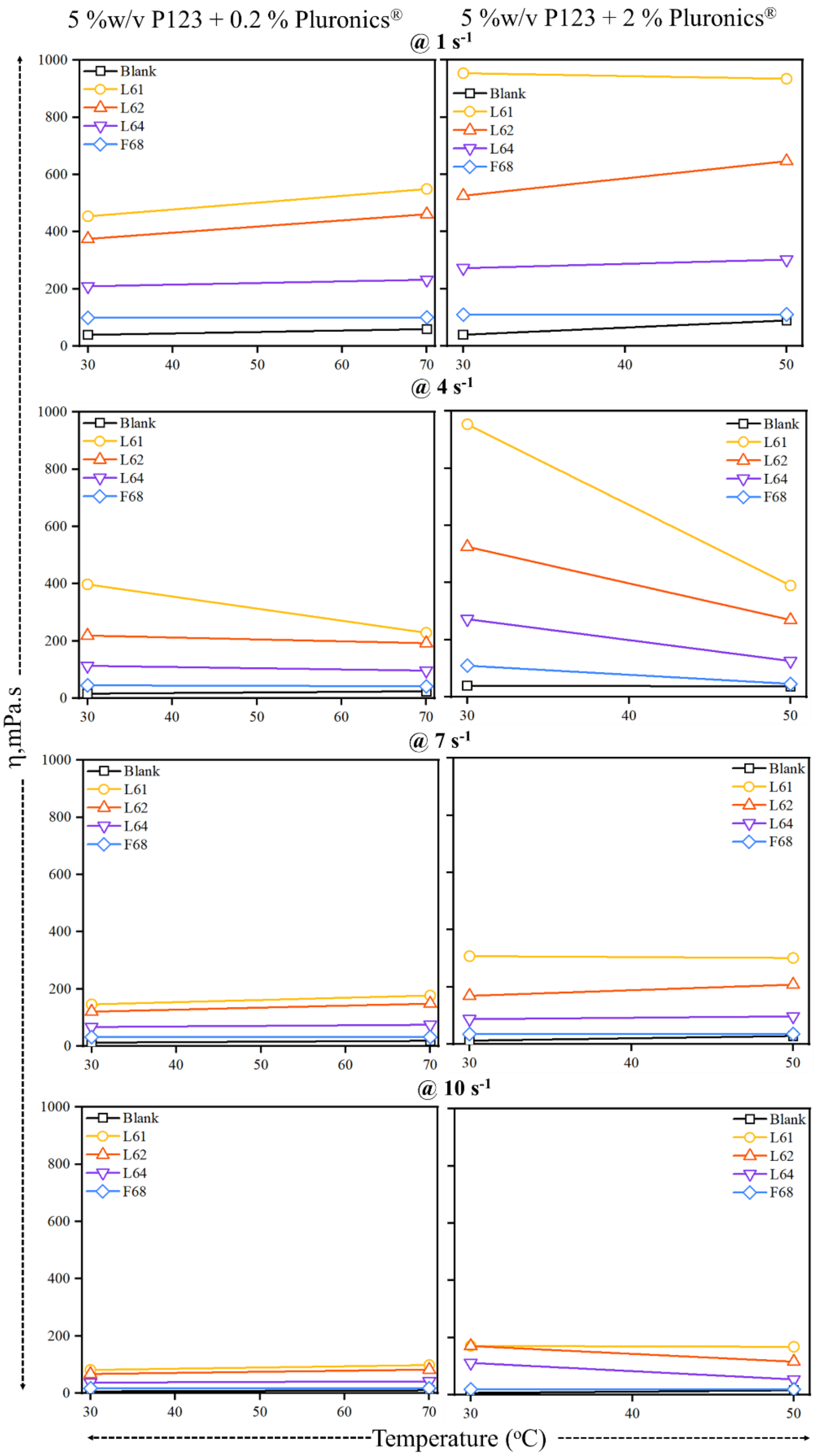

Figure S9: Apparent viscosity (η) of 5 %w/v P123 mixed with 0.2 % and 2 % Pluronics® at different temperatures and at different shear rates.

CG-MD simulation

Figure S10 shows the consolidated density profiles of the solutions shown in **Figures 6** and **7** of the main manuscript. **Figure S10a** compares the density profiles of P123 micelles and the arrangement of L61 moieties at 30 ºC and 70 ºC.

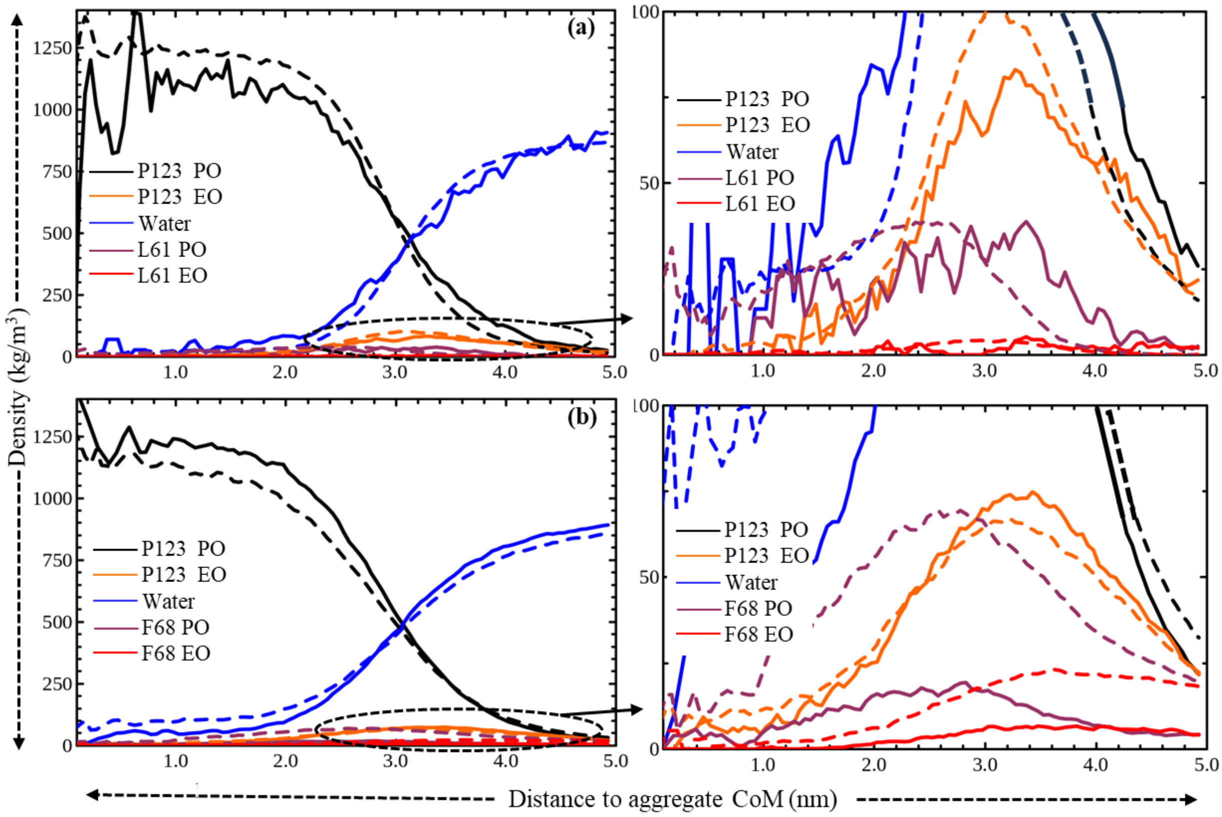

Figure S10: Micelle density profile comparison at 30 ºC (solid lines) and 70 ºC (dashed lines) for the 5 %w/v P123 solution with (a) 0.2 % of L61, and (b) 0.2% of F68. Figures at the right denote a zoomed view at the P123 micelle surface.

Very similar structures were found, but a swollen P123 micelle core at 70 ºC can be noticed by the increase in density of the P123 PO groups (black dashed line). The enhanced view of the micelle surface denotes that L61 moieties at 70 ºC were arranged slightly deeper when compared with the solution at 30 ºC. This can be noted by the relative position between PO groups at both temperatures (magenta solid and dashed lines for 30 ºC and 70 ºC, respectively). Similar micelles can be observed in the solution with F68 at both temperatures, as shown in **Figure S10b**. As mentioned earlier, EO groups of F68 moieties at 70 ºC seemed to be more solvated than at 30 ºC. If one compares the density profiles of F68 at the P123 micelle surface shown in the enlarged figure, the arrangement of F68 PO groups was similar (magenta lines) at both temperatures, but F68 EO groups at 70 ºC were flatter and more extended (red dashed line) when compared with their counterparts at 30 ºC, clearly pointing that the temperature facilitated the solvation of F68 moieties even when absorbed by P123.

Diffusion dynamics

The diffusion coefficient (D) is a parameter that quantifies the rate at which particles (such as molecules, atoms, or micelles) spread out over time due to random thermal motion. It is a central concept in molecular transport and gives insight into how fast molecules move and interact with their environment.

In molecular terms, the D is defined by Fick's Law and is related to the mean squared displacement (MSD) of particles. Mathematically, it is expressed as:

$$D = \frac{1}{6}\frac{d}{dt}\langle r^2(t)\rangle \tag{8}$$

Where $\langle r^2(t)\rangle$ is the mean squared displacement of the particles at time t. $\frac{d}{dt}$ is the time derivative, and the factor 1/6 is for 3D systems.

Calculating the MSD from the trajectories of atoms or molecules in an MD simulation can determine how mobile or diffusive the particles are in the system. High values of D indicate that particles are moving quickly, which suggests a low-viscosity environment or weak interactions. Contrary, low D values indicate slow-moving particles, implying stronger interactions or a higher viscosity environment. In Pluronic micelles with hydrophobic PO cores, the D shows how fast the micelle cores diffuse in solution. This is crucial for understanding the stability, size, and dynamics of micelles. MD simulations allow us to examine the diffusion changes with temperature. Since thermal energy drives molecular motion, higher temperatures generally increase diffusion. Hydrogen bonding, van der Waals interactions, or confined spaces (like within micelles), these factors will reduce the D and give insights into molecular assembly or micelle stabilization. In this study, we obtained the D and MSD for 5 %w/v P123 at two temperatures, 30 ºC, and 70 ºC, as shown in **Figure 1h** of the main manuscript. Results demonstrate the expected increase in diffusion at higher temperatures, providing a key insight into the behavior of micelles under varying thermal conditions.

The MSD values are initially small (2.26 $Å^2$ at 10 ns) but progressively increase, reaching 45.24 $Å^2$ by 500 ns. The trend of increasing MSD indicates that the PO groups in Pluronic P123 are undergoing diffusive motion. The D [P123_PO] = 0.0116×10^{-5} cm^2/s ± 0.0035×10^{-5} cm^2/s defines the rate at which the PPO groups in P123 are diffusing through the medium. In the initial stages, up to 100 ns, MSD values increase almost linearly with time, reflecting a steady diffusive motion. Above 100 ns, the MSD still increases but slower, suggesting that inter-micelle interactions became relevant. The constant increase in MSD over time indicates diffusive behavior, where the particles are not bound or constrained significantly, allowing them to spread out due to random thermal motion. However, the MSD values here are significantly higher than those at 30 °C for the same time intervals at 10 ns; the MSD is 3.56 $Å^2$ (compared to 2.26 $Å^2$ at 30 °C). By 500 ns, the MSD is 96.92 $Å^2$ (compared to 45.24 $Å^2$ at 30 °C). The increased MSD values reflect faster molecular movement at this elevated temperature. The higher diffusion coefficient at 70 °C, i.e., D[P123_PO] = 0.0338 × 10^{-5} cm^2/s ± 0.0249 compared to 30 °C, indicates that the PO groups are moving significantly faster at the higher temperature. This is expected, as increasing the temperature generally increases molecular motion and, thus, the diffusion rate. Up to 350 ns, the MSD increases consistently, indicating normal diffusion behavior (inter-micelle interactions). Above 350 ns, the increase in MSD slows down, though with slight fluctuations (e.g., between 84,469 $Å^2$ at 350 ns and 84,593 $Å^2$ at 360 ns). This may suggest some form of confinement or hindrance in motion, potentially due to crowding, micelle stabilization, or environmental constraints. After 370 ns, the MSD increases again, but with some irregularities, which could be related to thermal fluctuations or interactions within the system. As expected, the increase in temperature from 30 °C to 70 °C has caused the molecules (PO cores in P123) to diffuse more rapidly, reflected by higher MSD values and a larger diffusion coefficient. The error in the diffusion coefficient (±0.0249 × 10^{-5} cm^2/s) is larger than the data at 30 °C. This could indicate more variability in the diffusion process at higher temperatures, where the molecular motions are more energetic and less uniform. The slight fluctuation of MSD at the end of the simulation (after around 350 ns) could indicate the initial stages of the formation of vesicles, as observed in the simulation snapshots. The impact of a second Pluronic concentration in the micelle formation can be assessed throughout MSD and D of the PO core of P123 micelles at different temperatures, as depicted in **Figures S11a** and **S11b**.

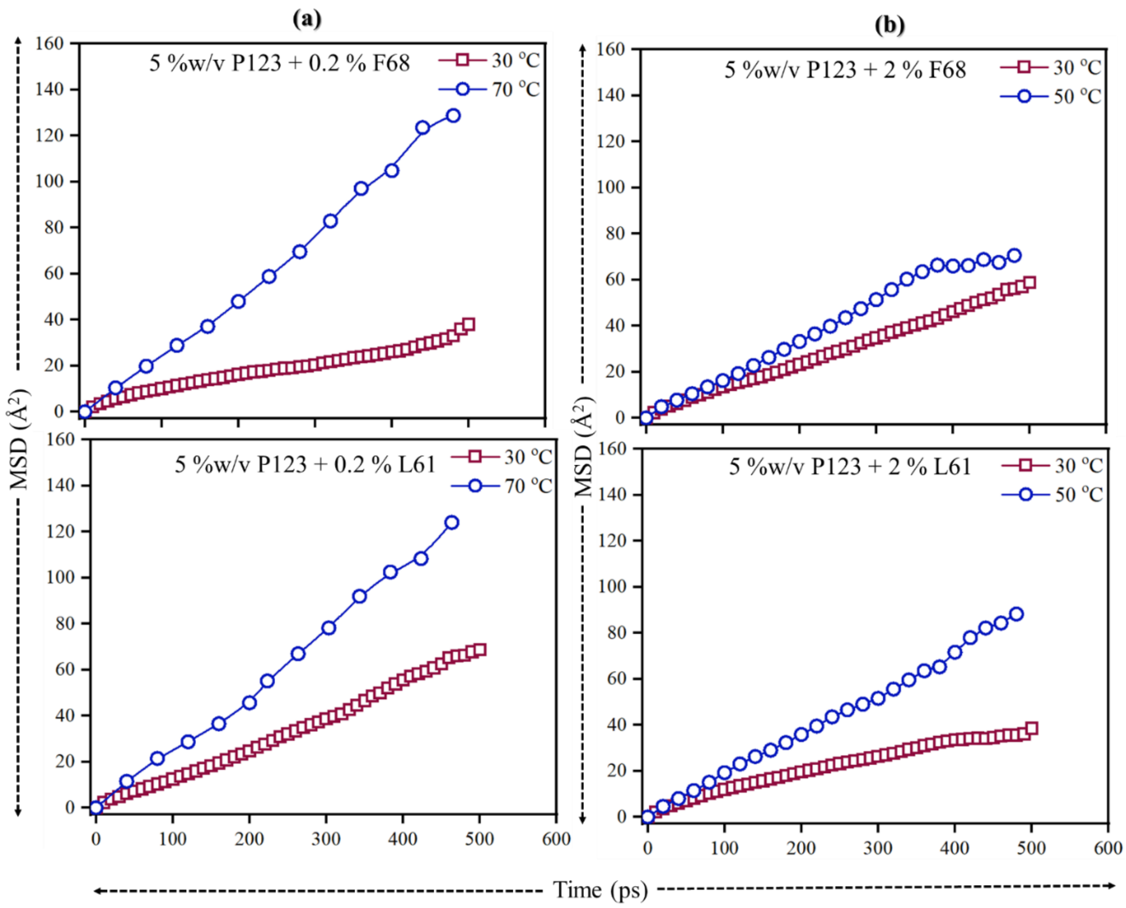

Figure S11: Comparative MSD profiles of PO cores in 5 %w/v P123 micelles with L61 and F68 with varying concentrations at various temperatures.

At 30 °C, the D for 0.2 % L61 in 5 %w/v P123 is ~0.0234×10^{-5} cm²/s ± 0.0058, indicating a relatively slow diffusion of P123 micelles in the presence of L61 (**Figure S11a**). At 10 ns, MSD is 2.30 Å² and increased to 12.52 Å² at 100 ns, and 24.79 Å² at 200 ns. This steady growth reflects normal diffusive behavior, with moderate molecular movement due to thermal motion. At 70 °C, the D increases significantly ~0.0442×10^{-5} cm²/s ± 0.0151. A higher D indicates much faster molecular movement of P123 micelles when temperature is raised (**Figure S11a**). MSD trend displays a noticeable increase, reflecting enhanced molecular mobility. At 40 ns, the MSD is 11.50 Å², increased to 45.67 Å² at 200 ns. At 500 ns, the MSD reaches 124.03 Å², denoting a significant shift compared to the values observed at 30 °C. This demonstrates that the increased thermal energy accelerates the diffusion process, enabling faster particle movement and creating more dynamic micellar structures.

In the case of 0.2 % F68 in 5 %w/v P123 at 30 °C, the diffusion is D ~ 0.008963×10^{-5} cm²/s ± 0.0009, exhibiting the slowest diffusion among the examined system, as depicted in **Figure S11a**. This suggests that P123 micelles have lower mobility at this temperature due to higher hydrophilicity of absorbed F68. The MSD values corroborate this, as they show a slower increase. At 10 ns, the MSD is 2.19 Å², increased to 10.12 Å² at 100 ns, which is lower than the L61 counterpart solution. By 200 ns, the MSD is 16.25 Å², indicating a slower diffusion rate than L61 since F68 moieties yield a more rigid and less dynamic environment for P123 micelles. At 70 °C, D increases significantly to ~ 0.0463 $\times 10^{-5}$ cm²/s ± 0.0113, similar to the L61 system. The relatively large increase in D denotes that, like L61, the P123 micelles in the presence of F68 denote much faster diffusion at elevated temperatures with MSD rapidly increasing. At 40 ns, the MSD is 10.43 Å², at 200 ns increased to 47.95 Å², displaying a much faster movement than at 30 °C. At 500 ns, MSD reaches 128.73 Å², comparable to the values observed for the L61 system at 70 °C. This demonstrates that higher temperatures significantly enhance molecular mobility in the presence of both L61 and F68.

In both L61 and F68 mixtures, the diffusion rates increase considerably at 70 °C, with L61 promoting slightly more dynamic motion at 30 °C. However, at 70 °C, the diffusion rates for both systems converge, indicating similar dynamics at higher temperatures.

At 30 °C, for 2 % L61 in 5 %w/v P123, the diffusion is D ~ 0.0117×10^{-5} cm²/s ± 0.0025, indicating moderate diffusion of P123 micelles in the blended system (**Figure S11b**). At 10 ns, the MSD is 2.20 Å², reaching 11.97 Å² by 100 ns and 19.58 Å² by 200 ns. This steady increase reflects a typical diffusive behavior with moderate molecular mobility. At 50 °C, the D increases significantly to ~ 0.0294×10^{-5} cm²/s ± 0.0017. This indicates much faster diffusion of P123 micelles at the higher temperature. The MSD values confirm this, showing a sharp increase. At 20 ns, the MSD is 4.62 Å², reaching 19.29 Å² by 100 ns and 35.86 Å² at 200 ns. This higher MSD reflects a much more dynamic system, with faster molecular movement driven by the added thermal energy.

For 2 % F68 in 5 %w/v P123 at 30 °C, D ~0.0185 × 10^{-5} cm^2/s ± 0.0023, indicating slightly faster diffusion than in the L61 system at the same temperature. MSD trend reflects this increased mobility. At 10 ns, the MSD is 2.32 $Å^2$, increased to 13.53 $Å^2$ at 100 ns and 23.24 $Å^2$ by 200 ns. The faster increase of MSD compared to the L61 system indicates that F68 promotes greater mobility at this temperature. At 50 °C, the D rises to ~ 0.0276 × 10^{-5} cm^2/s ± 0.0002, indicating a faster diffusion when the temperature is raised (**Figure S11b**). MSD denotes a notable, at 200 ns, is 4.87 $Å^2$, reaching 16.24 $Å^2$ by 100 ns and 33.20 $Å^2$ at 200 ns. This demonstrates a significantly faster molecular movement at 50 °C, similar to the L61 system.

P123 micelles with L61 or F68 exhibited significantly higher diffusion rates at 50 °C compared to 30 °C, consistent with increased molecular mobility at higher temperatures. At 30 °C, P123 micelles with F68 showed a slightly higher D and MSD when compared with the L61 mixture, suggesting a faster diffusion process at lower temperatures. At 50 °C, both systems exhibit similar diffusion rates and dynamic behavior, with high MSD values and fast molecular motion.

Scattering profile

DLS of 5 %w/v P123 was observed at 30 °C and 50 °C with different concentrations of Pluronics®. To visualize the effects of the temperature and the concentration of blended Pluronics® on the aggregation processes in P123 micelle, it was important to determine the size range of particles and to measure the magnitude of the interactions between the particles in the solution. This could lead to an understanding of the construction mechanism of particles in the solution as well as their dependence on the temperature and the concentration of additives.

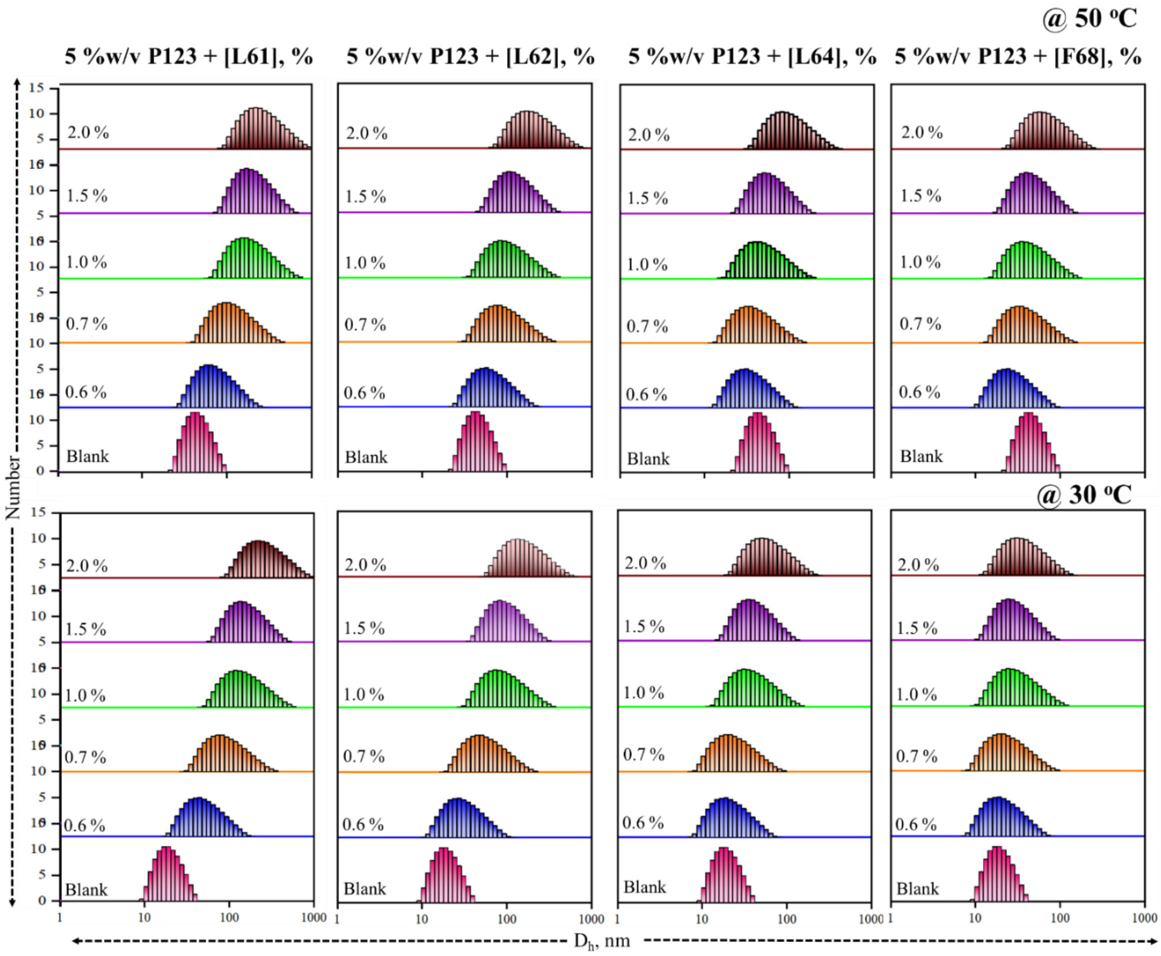

Figure S12: Temperature and concentration depend on the micellar size distribution of 5 %w/v P123 in the presence of Pluronics®.

The micellar sizes linearly increase with increasing concentration of blended Pluronics®. With increasing temperature, the micellar size grows again. This may be due to the incorporation of free PO blocks into the micelles and to the association of micelles in 'heaps' (aggregates of particles). The PO chains become more hydrophobic and can lead to two association mechanisms of the PO blocks. The first corresponds to the incorporation of free PO blocks in the core of the micelles, and the second corresponds to the association of two or more micelles with themselves, which can be depicted in the main manuscript of **Figures 6b** and **12b**. While in the presence of highly hydrophilic copolymers such as F68 at low temperature; the micelles were already hydrated and had a relatively higher D_h value. It is assumed that the growth of the size of the particles was due to the excluded volume effect that caused swelling of the micelles and also probably to the change of the spherical shape to an ellipsoidal form. The change to an ellipsoidal shape was assumed because it also represents the other different possible shapes of the micelles, such as spherical, rod-like, and disc-like; SANS has also observed the ellipsoidal shape for 5 %w/v P123 (**Table 1** of the main manuscript). It is known that the sphere-to-ellipse transition increases the η_{rel}, which agrees with our solution flow behavior measurements in this temperature range (**Figure 3** of the main manuscript).

CG-MD simulation

Figure S12 collages the consolidated density profiles of the solutions shown in **Figures 12** and **13** of the main manuscript. The comparative analysis of EO and PO blocks is conducted under varying temperature conditions.

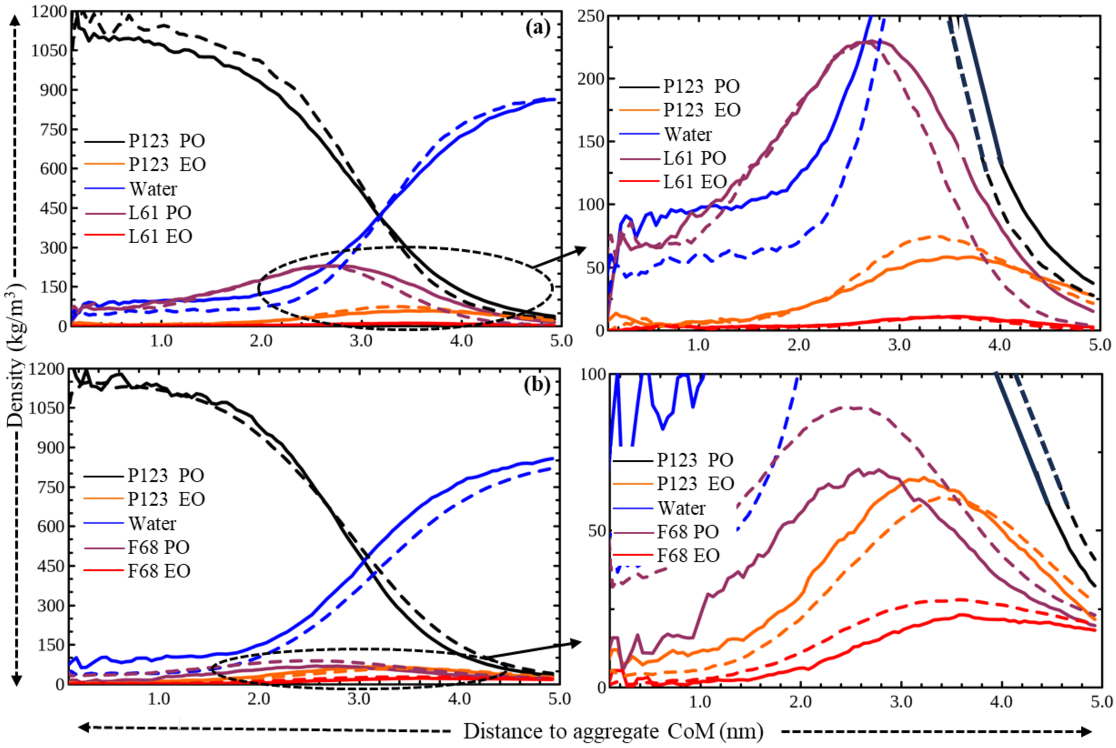

Figure S13: Micelle density profile comparison at 30 ºC and 50 ºC for the 5 %w/v P123 solution with (a) 2 % L61 and (b) 2 % F68. Figures at the right denote an enhanced view of the P123 micelle surface enclosed by the dashed black circle. The color code is the same as in **Figure 6** of the main manuscript.

Figure S13a compares the density profiles of P123 micelles and the arrangement of L61 moieties at 30 ºC and 50 ºC. Differ structures were found, but a swollen P123 micelle core at 50 ºC can be noticed from the increase in density of the P123 PO groups (black dashed line). The enhanced view of the micelle surface denotes that L61 moieties at 50 ºC were arranged slightly deeper when compared with the solution at 30 ºC. This can be noted by the relative position between PO groups at both temperatures (magenta solid and dashed lines for 30 ºC and 50 ºC, respectively). Similar micelles can be observed in the solution with F68 at both temperatures, as shown in **Figure 7** of the main manuscript. As mentioned earlier, EO groups of F68 moieties at 50 ºC seemed to be more solvated than at 30 ºC. If one compares the density profiles of F68 at the P123 micelle surface shown in the enlarged figure, the arrangement of F68 PO groups was similar (magenta lines) at both temperatures (**Figure S13b**), but F68 EO groups at 50 ºC were flatter and more extended (red dashed line) when compared with their counterparts at 30 ºC, clearly pointing that the temperature facilitated the solvation of F68 moieties even when absorbed by P123.